AGU PUBLICATIONS

JGR

Journal of Geophysical Research: Planets

RESEARCH ARTICLE

10.1002/2017JE005357

Key Points:
- Decameters of ice loss over the past 21 Myr form a sublimation lag, allowing Mars midlatitude ice sheets ~100 m thick to survive to present
- Retreat of this ice could have contributed 6% of the north polar layered deposits in the last 4 Myr and over 10% if polar deposits are older
- Modeling of vapor migration suggests that ice porosity can be sustained on timescales longer than retreat, consistent with radar observations

Correspondence to:
A. M. Bramson,
bramson@lpl.arizona.edu

Citation:
Bramson, A. M., Byrne, S., & Bapst, J. (2017). Preservation of midlatitude ice sheets on mars. *Journal of Geophysical Research: Planets*, *122*, 2250–2266. https://doi.org/10.1002/2017JE005357

Received 31 MAY 2017
Accepted 5 OCT 2017
Accepted article online 11 OCT 2017
Published online 9 NOV 2017

Preservation of Midlatitude Ice Sheets on Mars

A. M. Bramson[1], S. Byrne[1], and J. Bapst[1,2]

[1]Lunar and Planetary Laboratory, University of Arizona, Tucson, AZ, USA, [2]Department of Earth and Space Sciences, University of Washington, Seattle, WA, USA

Abstract Excess ice with a minimum age of tens of millions of years is widespread in Arcadia Planitia on Mars, and a similar deposit has been found in Utopia Planitia. The conditions that led to the formation and preservation of these midlatitude ice sheets hold clues to past climate and subsurface structure on Mars. We simulate the thermal stability and retreat of buried excess ice sheets over 21 Myr of Martian orbital solutions and find that the ice sheets can be orders of magnitude older than the obliquity cycles that are typically thought to drive midlatitude ice deposition and sublimation. Retreat of this ice in the last 4 Myr could have contributed ~6% of the volume of the north polar layered deposits (NPLD) and more than 10% if the NPLD are older than 4 Myr. Matching the measured dielectric constants of the Arcadia and Utopia Planitia deposits requires ice porosities of ~25–35%. We model geothermally driven vapor migration through porous ice under Martian temperatures and find that Martian firn may be able to maintain porosity for timescales longer than we predict for retreat of the ice.

1. Introduction

In the last decade, many lines of evidence have emerged suggesting that excess ice (ice that exceeds the pore volume of the regolith; also referred to as massive ice in terrestrial literature) is common in the northern midlatitudes (~30–60°N) of Mars. Shallow Radar (SHARAD) sounding of the subsurface has detected dielectric interfaces that have been attributed to the bottom of excess ice sheets in Arcadia Planitia (Bramson et al., 2015) and Utopia Planitia (Stuurman et al., 2016) decameters below the surface (Figure 1). Geomorphological evidence includes sublimation-thermokarst features, which form from collapse of the surface after localized sublimation of 5–10 m of excess ice, such as expanded craters (Viola et al., 2015) and scalloped depressions (Dundas, Byrne, & McEwen, 2015). The most definitive evidence for midlatitude buried excess ice in the Mars Odyssey Neutron Spectrometer (MONS) data was found to be in Arcadia Planitia (Feldman et al., 2011). Improved spatial resolution maps of epithermal neutron data from MONS also show that the near subsurface of Arcadia Planitia is hydrogen-rich (Wilson et al., 2018). Many new impacts expose and excavate nearly pure water ice (<10% dust by volume) as far south as 38°N (Dundas et al., 2014) within the uppermost meter, and craters across this region exhibit a terraced morphology due to layers in the subsurface that have been attributed to the same ice layer inferred to cause the dielectric interfaces in SHARAD data (Bramson et al., 2015).

The thicknesses measured for the Arcadia Planitia ice are 30–80 m, with the deeper values occurring near the southern extent of the deposit (~38–40°N). Based on a morphological unit of layered mesa terrain, the Utopia Planitia deposit was found to be 80–170 m in thickness. Both Arcadia and Utopia deposits, each containing ice volumes on the order of tens of thousands of cubic kilometers, were found to have dielectric constants (real part) of ~2.5 (Bramson et al., 2015; Stuurman et al., 2016), consistent with porous ice with low dust contents (Table 1). Because of the thick and widespread nature of these deposits, as well as the low dust contents and relatively high porosities suggested by the dielectric constants, snowfall is the most likely mechanism for their emplacement (Bramson et al., 2015).

The observed minimum age of the midlatitude excess ice in Arcadia Planitia was determined through crater-age dating to be tens of millions of years (Viola et al., 2015). This age has been difficult to reconcile with the standard paradigm of midlatitude ice, which generally interprets midlatitude ice as young ice that exchanges and equilibrates with the atmosphere to interact with the polar volatile reservoirs over Mars' 120 kyr periodicity obliquity cycles (e.g., Schorghofer, 2007). Experiments on the diffusive properties of Martian regolith, along with numerical simulations of the diffusion process, indicate that water vapor should readily diffuse from the subsurface (Bryson et al., 2008; Chevrier et al., 2007; Hudson et al., 2007; Sizemore & Mellon, 2008). This suggests that even brief excursions through periods of ice instability should have caused midlatitude ice to readily sublimate, and any replenishment of the ice from the atmosphere would be pore-filling rather

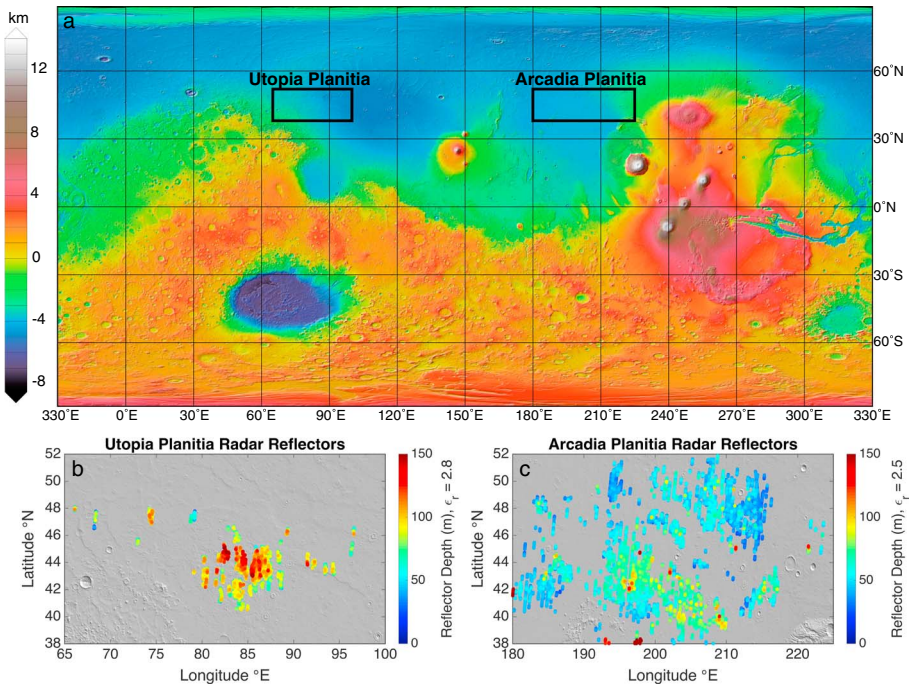

Figure 1. Map of midlatitude ice deposits discussed in text. (a) MOLA colorized elevation basemap with outlines of the regions of interest, shown in Figures 1b and 1c. (b) SHARAD subsurface reflectors in Utopia Planitia from Stuurman et al. (2016) and (c) Arcadia Planitia from Bramson et al. (2015). Figures 1b and 1c show reflector delay times converted to depth assuming a dielectric constant of 2.8 (Figure 1b) or 2.5 (Figure 1c) based on the respective studies cited for each region.

than excess ice. Both Schorghofer and Forget (2012) and Head et al. (2003) predict that an ice sheet would be geologically young (less than a few millions of years old) and should be actively retreating toward equilibrium under current atmospheric conditions. For example, a 30 m thick ice layer deposited 4.5 Ma (an order of magnitude younger than predicted for the ice observed in Arcadia Planitia) is not expected to survive to the present day in the midlatitudes (Schorghofer & Forget, 2012). Furthermore, the dielectric constants reported by Bramson et al. (2015) and Stuurman et al. (2016) both unexpectedly require substantial porosity in the excess ice layer. Densification models of the north polar layered deposits (NPLD) by Arthern, Winebrenner, and Waddington (2000) showed that under current polar conditions, ice very close to the surface is likely to have minimal porosity. Moreover, terrestrial firn typically densifies rapidly over timescales of hundreds to thousands of years (Cuffey & Paterson, 2010).

These discrepancies between our understanding of the stability and state of midlatitude ice and observations of old (tens of millions of years) excess porous ice at these latitudes can inform us about Mars' climatic history and subsurface structure. Identifying the conditions that led to the present-day distribution of excess ice is important for future resources that will support human exploration as well as understanding: (a) the stability

Table 1
Observations of Ice Deposits in Arcadia Planitia (Bramson et al., 2015) and Utopia Planitia (Stuurman et al., 2016), and TES-Derived Thermal Inertias From Putzig et al. (2005) and Albedos From Christensen et al. (2001)

Regional observational constraints of excess ice deposits		
Deposit properties	Arcadia Planitia	Utopia Planitia
Latitude range	38–52°N	40–50°N
Dielectric constant	2.5 ± 0.28	2.8 ± 0.8
Thickness	30–80 m	80–170 m
Area	250,000 km^2 (radar reflective region)– 1,200,000 km^2 (convex hull of radar reflections)	375,000 km^2 (radar reflective region)–1,000,000 km^2 (entire morphological unit)
Volume	13,000 km^3–61,000 km^3	8,400–14,300 km^3
Thermal inertia of the region	196 J m^{-2} K^{-1} $s^{-0.5}$	195 J m^{-2} K^{-1} $s^{-0.5}$
Albedo of the region	0.23	0.12

Table 2
Parameters Used in the Thermal Model and Ice Retreat Calculations of Equations (1)–(4)

Variable	Parameter	Comment
ε	emissivity of the surface	assumed to be 1, or 0.8 if covered in CO_2 frost
σ	Stefan-Boltzmann constant	5.67×10^{-8} W m^{-2} K^{-4}
T_{surf}	surface temperature	calculated at every time step
S_o	solar flux at Mars	calculated at every time step throughout a Martian year using the planet's orbital properties and a rotation rate of 88775.2 s; includes an additional 2% of the top-of-atmosphere flux as scattered light
i	incidence angle of sunlight	calculated based on latitude and can include the effects of sloped terrain
A	surface albedo	0.23 for Arcadia Planitia, 0.12 for Utopia Planitia, and 0.65 if the surface is covered in CO_2 frost
L_{CO2}	latent heat of CO_2 frost on the surface	590 kJ kg^{-1}
m_{CO2}	mass of a CO_2 surface layer	calculated at every time step; generally ranges from 0 to ~45 kg m^{-2} depending on the latitude and time of the year
k	thermal conductivity	see Table 3
$IR_{\downarrow}$	downwelling infrared radiation from the atmosphere	assumed to be 4% of the noontime insolation
I	thermal inertia	see Table 3
ρ	density	see Table 3
c	heat capacity	see Table 3
D_{reg}	vapor diffusion coefficient through the regolith	nominal value of 3×10^{-4} m^2 s^{-1} from Dundas et al. (2015), consistent with Hudson et al. (2007)
D_{ice}	vapor diffusion coefficient through porous ice	nominal value of 10^{-4} m^2 s^{-1}
$\overline{\rho}_{vapor}$	annual average saturation vapor density	calculated for each orbital solution
$\overline{\rho}_{atmos}$	annual average atmospheric water vapor density	calculated for each orbital solution, see section 2.2
z_i	depth to ice stability when it is between the surface and z_{ei}	occurs where $\overline{\rho}_{vapor} = \overline{\rho}_{atmos}$
z_{ei}	depth to top of the excess ice interface	increases over time as ice retreats and leaves behind a lag deposit
ϕ_{reg}	porosity of the regolith layer	
ϕ_{ice}	porosity of the excess ice layer	
d	volumetric dust content of the excess ice layer	
ρ_{ice}	density of pure water ice	917 kg m^{-3}

of ice in the Amazonian (3 Ga to present), (b) the subsurface structure in the midlatitudes, and (c) the orbital forcing of the Martian climate. To test conditions for excess ice preservation in the last tens of millions of years, we calculated the expected ice retreat throughout 21 Myr long orbital solutions (obliquity, eccentricity, and longitude of perihelion; Laskar et al., 2004). We used 1-D thermal conduction and vapor diffusion models to characterize the conditions necessary to reproduce the observed thicknesses and dielectric constants of excess ice deposits and assess if it is reasonable to expect long-term stability of porous midlatitude excess ice.

2. Methods

2.1. Thermal Model

We calculate temperatures of the subsurface using a 1-D thermal conduction model, which follows the surface energy balance of equation (1), with thermal conduction between numerical layers in the subsurface (equation (2)) as employed in other such models (Chamberlain & Boynton, 2007; Kieffer, 2013; Mellon et al., 2000; Putzig & Mellon, 2007; Schorghofer, 2007; Schorghofer & Aharonson, 2005; Vasavada, Paige, & Wood, 1999). The model solves the heat equation using a semi-implicit Crank-Nicolson numerical scheme (Crank & Nicolson, 1947) and assumes that the surface is in energetic equilibrium while the bottom boundary condition

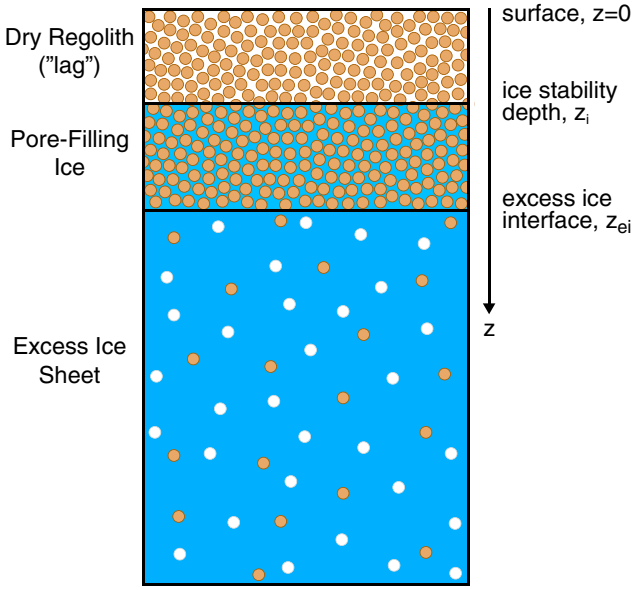

Figure 2. Stratigraphy of thermophysical layers modeled in the case where pore-filling ice is present.

is a 30 mW/m^2 geothermal heat flux (Fanale, 1976). A description of each parameter in these and later equations can be found in Table 2.

$$\varepsilon\sigma T_{surf}^4 = S_o\cos(i)(1-A) + L_{CO2}\frac{dm_{CO2}}{dt} + k\frac{\partial T}{\partial z} + IR_{\downarrow} \quad (1)$$

$$\rho c\frac{\partial T}{\partial t} = \frac{\partial}{\partial z}\left(k\frac{\partial T}{\partial z}\right) \quad (2)$$

The parameter t is the variable time, z is the vertical coordinate representing depth, and T represents the temperature within a given layer. The term containing m_{CO2} accounts for the presence of a surface layer of carbon dioxide frost when surface temperatures fall below the frost point of CO_2, ~148 K for 610 Pa of atmospheric pressure. When this occurs, the surface temperature is fixed at the frost point, which is calculated for each time of the year using a curve fit to Viking 1 atmospheric pressure data (Hess et al., 1980). We used an average albedo for each area of interest, 0.23 for Arcadia Planitia and 0.12 for Utopia Planitia, based on Thermal Emission Spectrometer (TES) data (Christensen et al., 2001). The calculation of solar flux also includes an additional 2% of the top-of-atmosphere flux as an approximation for atmospherically scattered visible light (Aharonson & Schorghofer, 2006; Kieffer et al., 1977). We model the downwelling infrared radiation as 4% of the daily noontime flux (Aharonson & Schorghofer, 2006).

Layer thickness is calculated such that 15 numerical layers are present within one diurnal skin depth of the regolith. The thickness of each layer grows by 3% so that layers are thinnest near the surface, where the temperature fluctuations are greatest, allowing these fluctuations to be resolved. The model domain extends to six annual skin depths. The model uses a numerical time step of 1,500 s, though we also tested time steps of 500 and 1,000 s to ensure this choice affected results to <0.5%. After running a "wind-up" phase of five Martian years, we set temperatures at all depths equal to the annual average surface temperature. We then run the model for another 10 Martian years, recording annual averages at each depth in the last year of the run. The temperatures in this last year converge to within a tenth of a Kelvin of solutions from the year before it.

We allow for subsurface layers of different thermophysical properties, which we use to model a dry surface regolith layer of low thermal inertia that may contain ice within its pores (Figure 2). A dry "lag" deposit forms atop the excess ice upon its retreat and damps temperature oscillations, thus insulating the ice below. The regolith has some porosity (ϕ_{reg}), nominally 40%, and the excess ice is modeled with varying porosity (ϕ_{ice}) and volumetric dust content (d). We calculate volumetric heat capacity (ρc) of the layers using a linear combination of silicate material, ice and porosity. Example values for regolith with and without pore-filling ice, as well as the end member values of the rocky material and pure ice used in the calculation, are provided in Table 3. The conductivity of the upper, dry regolith layer is determined from the square of the thermal inertia divided by the volumetric heat capacity. The thermal inertias, based on analysis of nighttime TES temperatures (Putzig et al., 2005) for each region, are 196 J m^{-2} K^{-1} s$^{-0.5}$ for Arcadia Planitia and 195 J m^{-2} K^{-1} s$^{-0.5}$ for Utopia Planitia. The pore-filling ice and excess ice layer conductivities are calculated

Table 3
Thermophysical Properties: Rock and Ice End-Members and Values for Each Layer in the Nominal Arcadia Planitia Case

Property	Rock end-member	Ice end-member	Dry regolith (ϕ_{reg} = 40%; TI = 196 J m^{-2} K^{-1} s$^{-0.5}$)	Regolith (ϕ_{reg} = 40%) with pore-filling ice	Excess ice (ϕ_{ice} = 30%; d = 3%)
Conductivity, k (W m^{-1} K^{-1})	2	3.2	0.023	2.48	2.14
Heat capacity, c (J kg^{-1} K^{-1})	837	1,540	ρc = 1,657,260 kg s^{-2} K^{-1} m^{-1}	ρc = 2,223,980 kg s^{-2} K^{-1} m^{-1}	ρc = 1,032,119 kg s^{-2} K^{-1} m^{-1}
Density, ρ (kg m^{-3})	3,300	920			

assuming linear combinations of end-member conductivities based on volumetric contents of each component (rock, ice, and air) in the mixture. However, we compared our modeling results between runs using an ice conductivity with negligible dependence on porosity and that of the Van Dusen (1929) equation (equation (3)), which is nonlinear with density. The difference in the effective conductivity between these two schemes is a factor of up to 4–5 for our highest porosities (50%) and yields only a 2–3% change in the final ice retreat and lag thickness results. The effective conductivity of a mixture ultimately depends on how the two end-members mix with each other; alternative effective thermal conductivity mixing models include Series (Mellon, Jakosky, & Postawko, 1997), Parallel (Wechsler, Glaser, & Fountain, 1972), Geometric Mean (Johansen, 1975), and Volumetric (Siegler et al., 2012). Experiments on icy Martian regolith analogs show that the relationship will depend on the geometry of contacts between grains (Piqueux & Christensen, 2009b; Siegler et al., 2012).

$$k = 2.1\times10^{-2} + \left(4.2\times10^{-4}\right)\rho + \left(2.2\times10^{-9}\right)\rho^3 \tag{3}$$

Pore-filling ice is stable when the annual average water-vapor density at or above the excess ice interface (z_{ei}) is less than or equal to the atmosphere, $\overline{\rho}_{vapor} \leq \overline{\rho}_{atmos}$ (Schorghofer, 2010). Using modeled temperatures with the Clausius-Clapeyron equation and ideal gas law, we calculate vapor densities throughout the regolith and (if it exists) we find the stability depth (z_i) where $\overline{\rho}_{vapor} = \overline{\rho}_{atmos}$. We assume that the pore-filling ice is always in equilibrium with the atmosphere and that regolith pores below the stability depth (between z_i and z_{ei}) are always completely filled with ice (model stratigraphy shown in Figure 2). Supporting these assumptions are experiments on the diffusivity of Mars regolith simulants, which suggest rapid removal and emplacement of pore ice on timescales comparable to periodic changes in obliquity (120 kyr) (Hudson et al., 2007). If pore-filling ice exists within the lag deposit, we assume that it is impermeable and so there is no retreat of the excess ice sheet below.

No pore-filling ice is stable when z_i exceeds z_{ei}. In this case there is only dry regolith atop the excess ice and vapor from the excess ice can diffuse away through the open pores. When $\overline{\rho}_{vapor} > \overline{\rho}_{atmos}$ at the excess-ice interface, ice is lost at a rate that is dependent on the vapor diffusion coefficient of the regolith, the difference between the vapor density and atmospheric vapor content, and the depth of z_{ei} (equation (4)). The diffusion coefficients for a range of materials under simulated Mars surface conditions were found to be $\sim 2\times10^{-5}$ m^2/s $- 5\times10^{-4}$ m^2/s (Hudson et al., 2007); we use a nominal value of $D_{\mathrm{reg}} = 3\times10^{-4}$ m^2/s. When excess ice retreats, it leaves behind any silicate material embedded within it, thus growing the lag deposit and increasing z_{ei}. We implement the growth of this regolith layer over time following the method described in Schorghofer (2010) and using his integrated solution for lag thickness. Lag thickness changes within each time step, and we use the average lag thickness from the start and end of the orbital time step when calculating the ice retreat for that orbital solution (equation (4)). We assume that the excess ice sheet is of infinite thickness in order to evaluate how much ice loss would be expected over time. We step through the 21 Myr of orbital solutions in 10 kyr increments. Using a maximum resolution of 1 kyr instead caused the final lag and ice retreat thicknesses to differ by only tenths of a percent.

$$\mathit{Ice\ Retreat} = \frac{D_{reg}\left(\overline{\rho}_{vapor,Zei} - \overline{\rho}_{atmos}\right)\Delta \mathrm{t}}{\overline{z}_{ei}\left(1 - \phi_{ice} - \mathrm{d}\right)\rho_{ice}} \tag{4}$$

Because we wish to estimate ice retreat over millions of years, we use the fast numerical method developed by Schorghofer (2010), in which the annual time-averaged calculations are sufficient for calculating long-term evolution of subsurface ice while offering an improvement in runtime by 5 orders of magnitude. Although our thermal model resolves diurnal temperatures variations which are subsequently applied to calculations of the annual average vapor densities, it would be impractical (>1,000 year runtimes) to simulate ice exchange at a similar time step. Therefore, our model ignores processes involved with the daily and seasonal exchange of water between the atmosphere and regolith. Schorghofer (2010) shows that while the strategy does not correctly reproduce seasonal subsurface ice, it does correctly predict the amount of perennial ice.

2.2. Free Parameters Tested

Given the importance of $\overline{\rho}_{atmos}$ on ice stability conditions, we run the model using various schemes from the literature that describe how $\overline{\rho}_{atmos}$ varies over time. Our nominal case uses the results of Schorghofer and Forget (2012) ("SF12"), which provides atmospheric partial pressure of H_2O versus obliquity, which we convert to vapor density using the annual average surface temperature outputted by the model.

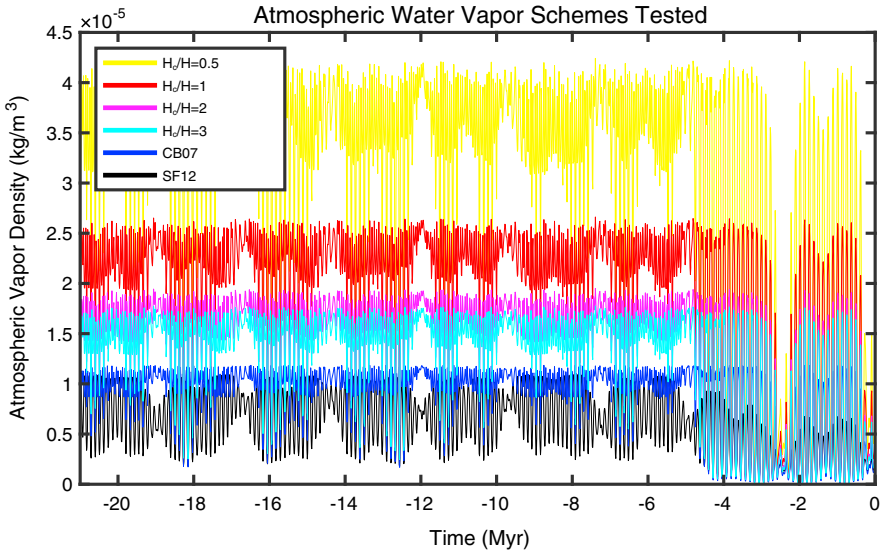

Figure 3. Obliquity-dependent atmospheric vapor densities on the surface (45°N) over time in the six different schemes tested. SF12 stands for the scheme in Schorghofer and Forget (2012); CB07 represents that of Chamberlain and Boynton (2007); H_c/H schemes are based on the results of CB07 but are converted to vapor densities using a factor of condensation height relative to atmospheric scale height.

We also ran cases using the results of Chamberlain and Boynton (2007) ("CB07"), which yield a global average 100 precipitable micrometers (pr μm) of water vapor in the atmosphere at high obliquities, fractions (thousandths to tenths) of a pr μm at low (10°–15°) obliquities, and about 20 pr μm of globally averaged atmospheric water vapor at the present obliquity. We fit a curve to the CB07 results in 5° increments for obliquities 10–45°, and then converted precipitable micrometers to water vapor density in the same manner as CB07 (i.e., by assuming a constant mixing ratio throughout the whole atmosphere). This yields vapor densities larger than Schorghofer and Forget (2012) except at extremely low obliquities ($<$17°).

We also converted the fit to the CB07 results to surface water vapor densities using condensation height (H_c) to atmospheric scale height (H) ratios (Schorghofer & Aharonson, 2005) of 0.5, 1, 2, and 3 and multiplying by an elevation correction term of $e^{-\frac{z}{H}}$ (Mellon, Feldman, & Prettyman, 2004; Schorghofer & Forget, 2012). This elevation term increases surface water vapor density by ~33% relative to that at 0 km for an elevation of -3 km (the value we assume for the northern plains) and an atmospheric scale height of 10.8 km (which we leave constant throughout all model runs). We assume that the atmosphere is evenly mixed below the altitude specified by H_c. Changing this value affects the concentration of water vapor near the surface (e.g., lower H_c/H concentrates water vapor lower in the atmosphere) and allows us to test the effect of surface concentration on expected ice retreat. The resulting water vapor densities at each orbital solution for each scheme that we test are shown in Figure 3. While these schemes are among those offered in the current literature, they assume the presence of the NPLD, and it is unclear if these schemes would still hold during higher obliquities in the absence of polar volatile reservoirs.

The porosity and dust content of the excess ice affect the results by changing the thickness of ice lost and the rate of thickening of the lag deposit. Higher porosities lead to increased ice retreat for a given mass flux, while increased dust content in the ice leads to a faster buildup of the lag, thereby increasing the insulation of the excess ice and reducing subsequent ice retreat. These properties also have the greatest influence on the expected dielectric constant of the subsurface stratigraphy. Therefore, we explore the parameter space of porosities and dust contents that produce final model stratigraphies that match the observed dielectric constants (Table 1).

2.3. Calculating Dielectric Constants From Model Output

We calculate the real part of the dielectric constants (also commonly referred to as the relative permittivity), ε_r, for the final model stratigraphies (dry lag with possible pore-filling ice layer atop excess ice) of each model run using the dielectric mixing model of Stillman, Grimm, and Dec (2010). This mixing model was also used to

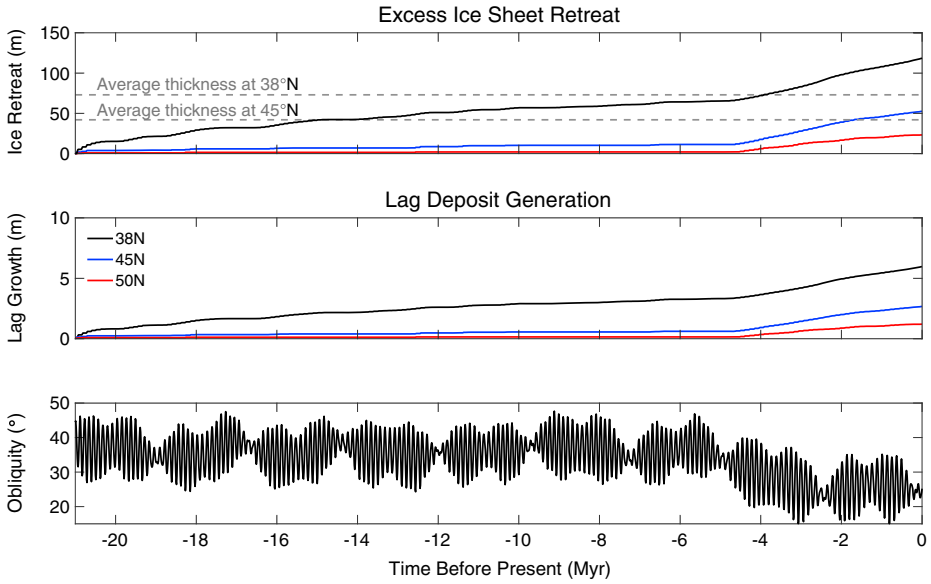

Figure 4. Modeled ice retreat and lag deposit growth over time for the latitude range of excess ice in Arcadia Planitia using the nominal case of 30% ice porosity and 3% ice dust content. The grey dashed lines in the top plot show the average thickness of the Arcadia Planitia ice sheet at 38°N and 45°N based on the radar measurements in Bramson et al. (2015).

relate dielectric constants to composition in Bramson et al. (2015) and Stuurman et al. (2016). We use this power law relationship (equation (5)) to calculate the dielectric constant for each of the three thermophysical layers (ε_N) of a given volumetric fraction (v) of rock, air, and ice, assuming ε_{rock} = 8, ε_{ice} = 3.15, and ε_{air} = 1. In the dry regolith layer, $v_{rock} = 1 - \phi_{reg}$, $v_{air} = \phi_{reg}$, and v_{ice} = 0. For pore-filling ice, v_{rock} is the same as the dry regolith case, but $v_{ice} = \phi_{reg}$ and v_{air} = 0. Within the excess ice, $v_{rock} = d$, $v_{air} = \phi_{ice}$, and v_{ice} = 1-d-ϕ_{ice}. For our nominal case, this mixing model yields a dielectric constant of 4.16 for dry regolith, 5.72 for pore-filling ice, and 2.43 for excess ice.

$$\varepsilon_N^{1/2.7} = v_{rock}\varepsilon_{rock}^{1/2.7} + v_{ice}\varepsilon_{ice}^{1/2.7} + v_{air}\varepsilon_{air}^{1/2.7} \quad (5)$$

$$\Delta t_N = \frac{\Delta z_N \sqrt{\varepsilon_N}}{v_c} \quad (6)$$

$$\varepsilon_r = \left(\frac{v_c \sum_{N=1}^{3} \Delta t_N}{z_{total}}\right)^2 \quad (7)$$

We calculate the time it would take a radar wave to travel through each layer, Δt_N (equation (6)), using the thicknesses of each layer (Δz_N) outputted by our ice stability model at the final time step (present day) for the lag and pore-filling layers, and the currently observed depths to the bottom of the excess ice (z_{total}). We then set the ratio of z_{total} over the total delay time to the bottom of the stratigraphy equal to the ratio of the speed of light (v_c) over the square root of the dielectric constant. Solving for the bulk dielectric constant of the total stratigraphy gives equation (7).

In this calculation, we use observations of the bottom of the excess ice sheet today (and thus the depth of the total modeled stratigraphy, z_{total}) at 42 m at 45°N and 73 m at 38°N in Arcadia Planitia. We use an average thickness of 100 m for the Utopia Planitia deposit (Stuurman et al., 2016) to calculate a dielectric constant for the final modeled stratigraphies for our Utopia Planitia model results.

3. Results

Starting with an infinitely thick excess ice sheet buried by dry regolith such that the top of the excess ice is at the equilibrium depth ($z_{ei} = z_i$) for conditions 21 Myr ago, we calculate how much retreat the ice would undergo to the present day. At 45°N, this leads to an initial stratigraphy of 4.7 cm of dry regolith atop the excess ice. Meanwhile, the thickness of the initial regolith layer is 5.6 cm at 38°N and 4.6 cm at 50°N. Our

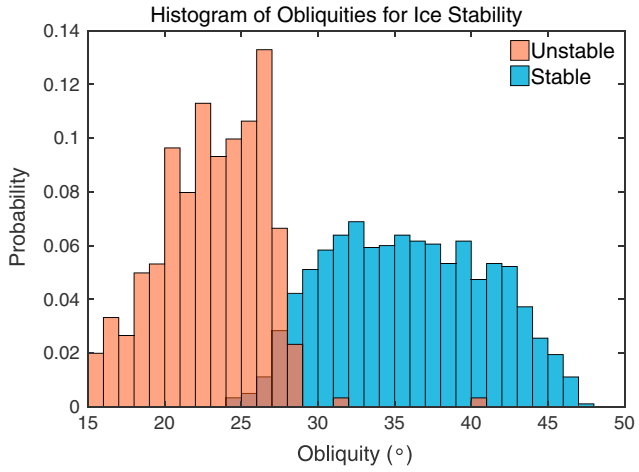

Figure 5. Distribution of obliquities in the last 21 Myr when ice is unstable (orange) and stable (blue) for our nominal case at 45°N.

nominal case includes 30% ice porosity and 3% ice dust content at 45°N in Arcadia Planitia. The nominal case also assumes the SF12 atmospheric surface water vapor density scheme.

The amount of total retreat is of the same order of magnitude as the observed thicknesses of ice in Arcadia Planitia and Utopia Planitia today (Figure 4), suggesting that it is reasonable to preserve tens to hundreds of meters of ice over time frames of tens of Myr, as it would only require an initial ice sheet 2–3 times thicker than present. Most ice loss occurs during times of low obliquity, as this is when the midlatitudes receive the most direct solar radiation, causing temperatures, and thus vapor densities at the excess ice interface, to be higher. Low obliquity is also the period with the driest atmosphere. We find that 24.36° is the lowest obliquity for which pore-filling ice is stable at 45°N. During any obliquity lower than this, ice is lost from the ice sheet.

Ice is lost at higher obliquities if the eccentricity and argument of perihelion are unfavorable for ice stability. Figure 5 shows a normalized histogram of obliquities for which ice is stable and unstable. The two outliers of ice instability at high obliquities are within the first 60 kyr of the run when the lag deposit is thinnest. Excluding those two points, the highest obliquity at which ice retreats is 28.94°. Therefore, ice is stable at any obliquity above this value except the two early cases.

About 4 Myr ago, the mean obliquity dropped from about 35° to 25° (Laskar et al., 2004). As shown in Figure 4, most ice retreat, especially at the middle to higher latitudes of those we consider, occurs within this time frame. At 38°N, roughly half of the retreat has occurred since this drop in average obliquity at around 4 Ma, the other half occurring in the much longer timespan (4–21 Myr). At 50°N, ~75% of the total retreat occurs since 4 Ma. Orbital solutions older than 21 Ma are chaotic, but if the average obliquity was similar to or higher than that between 4 and 21 Ma, then ice could be older without significantly increasing the total loss. Ice is less stable at lower latitudes, and we find that ice retreat is higher by a factor of 4 at the lowest latitudes (38°N) versus the highest latitudes (50°N) modeled. During the 21 Myr simulation, pore-filling ice is stable at 45°N 85.6% of the time and 95.3% of the time prior to 4 Ma. At 38°N, pore-filling ice exists 64.3% of the time overall and 74.8% of the time before 4 Ma.

During the last 4 Myr, our model predicts pore-filling ice to be stable 45% of the time, with retreat occurring during the other 55%. Our nominal model finds pore-filling ice stable as recently as 80 ka at a depth of 34 cm in Arcadia Planitia (45°N). At 38°N pore-filling ice was briefly stable at 380 ka below 35 cm of dry regolith and was only stable 20.3% of the time since 4 Ma. We find pore-filling ice to be stable at 50°N in the current climate at an equilibrium depth of 0.18 m, matching previous thermal model results for the present epoch (e.g., Chamberlain & Boynton, 2007).

The deposit in Arcadia Planitia extends at least as far south as 38°N where predicted losses are more than double those at 45°N (Figure 4); however, the excess ice mapped in these southern areas is approximately twice as thick as the northern areas (if the dielectric constant of 2.5 is the same across the deposit). Therefore, the higher losses at more southerly locations are still within a factor of 1–2 of the surviving ice thicknesses.

It may be feasible that the thermokarstically expanded craters across Arcadia Planitia (Viola et al., 2015) would not be substantially affected by significant ice loss if the ice loss in the crater occurs at the same rate as the surrounding plains during periods of retreat across the region. However, additional work is needed to determine the extent that the expanded craters' shape or even presence would be affected by slow retreat of the entire ice sheet. Additionally, removal of ice from the upper surface would not necessarily affect the location of terraces in craters across Arcadia Planitia (Bramson et al., 2015) that form at the ice-rock interface, as long as not all of the ice has been removed.

3.1. Effect of Atmospheric Water Vapor Content

For the atmospheric water vapor versus obliquity schemes tested (described in section 2.2), the final ice retreat varies by at most tens of percent (Figure 6). Lower H_c/H values act to concentrate atmospheric water vapor closer to the surface, increasing ice stability and leading to less ice retreat and growth of the lag deposit. For small

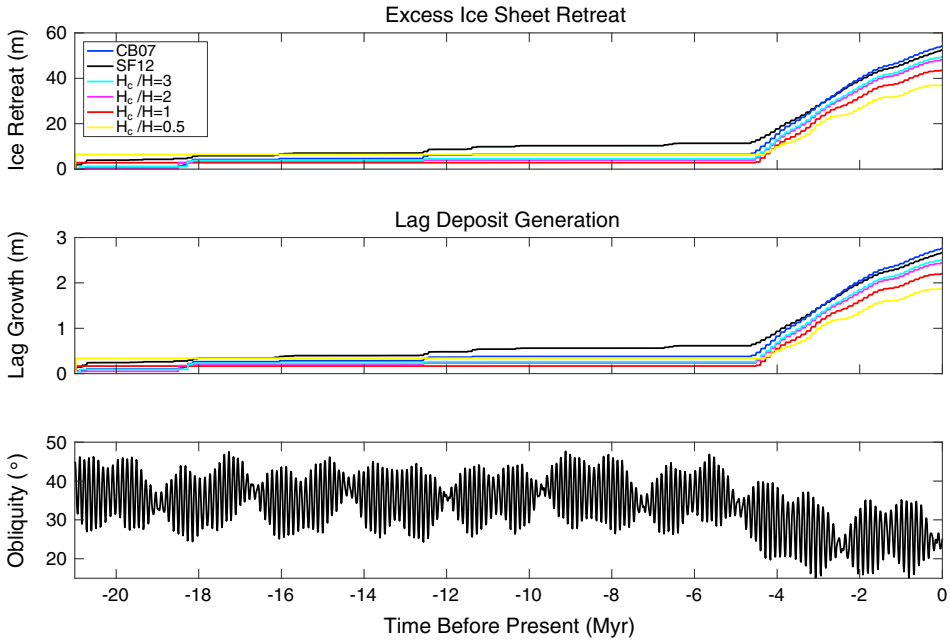

Figure 6. Modeled ice retreat and lag growth over 21 Myr for different atmospheric water vapor schemes at 45°N in Arcadia Planitia.

H_c/H values, ice becomes stable up to the surface. For H_c/H = 1/3, ice becomes stable within the vertical resolution of our top numerical layer. Because our model does not treat the processes involved with surface ice, we use a minimum H_c/H = 0.5, in which the shallowest equilibrium depth of pore-filling ice is 4 mm. With H_c/H = 0.5, pore-filling ice would be stable during the present epoch at 45°N at an equilibrium depth of 24 cm.

Temperature is a factor in computing the atmospheric water vapor densities in all of the schemes tested except CB07, which uses a constant mixing ratio throughout the entire atmosphere. Lower temperatures (and therefore higher latitudes) yield higher vapor densities. The vapor densities are therefore also sensitive to obliquity. SF12 produces the most ice retreat of all schemes at a latitude of 38°N but the least retreat at 50°N. At 45°N, SF12 and CB07 yield a similar amount of final ice retreat at the end of the 21 Myr run (Figure 6). But the relative amount of retreat between these schemes is not uniform over time: SF12 experiences the most sublimation between 21 and 4 Myr ago, and CB07 surpasses SF12 in the last 4 Myr when the mean obliquity is lower. This effect, however, does not change our conclusions for the latitude range we consider, and the atmospheric scheme only affects the final ice retreats by at most tens of percent.

3.2. Porosity and Dust Content of the Ice

We calculated the dielectric constants for the final modeled stratigraphies as described in section 2.3, testing a range of dust contents and porosities of the excess ice layer to match the dielectric constants measured for Arcadia Planitia (2.5 ± 0.28), shown in Figure 7. Some dust content is needed in the ice so that a lag deposit can form, though we find that dust contents below ~1% lead to more than 200 m of ice loss at 38°N and more than 100 m at 45°N (Figure 7, bottom row), making these cases less likely. However, higher dust contents lead to thicker lag deposits (Figure 7, middle row) and thus higher dielectric constants. Therefore, the most likely solution involves intermediate values of both dust content and porosity within the parameter space allowed by the dielectric constants. Ice porosities of ~25–35% and dust contents of ~1–5% are most likely to explain both the preservation of ice and match the measured dielectric constants (Figure 7). These dust contents are consistent with that expected for ice-rich Lobate Debris Aprons in the midlatitudes based on radar attenuation through these glacial features (dust fractions $<$ 10%) (Holt et al., 2008).

While the thermal inertia of Utopia Planitia is similar to that of Arcadia Planitia, the region is darker with an albedo 0.12 (compared to Arcadia Planitia's albedo of 0.23). For the same latitude (45°N), this has the effect of essentially doubling the amount of ice retreat and therefore lag growth (Figure 8). The calculated ice retreat is larger than the Arcadia Planitia cases, but the retreat is still of the same order of magnitude as

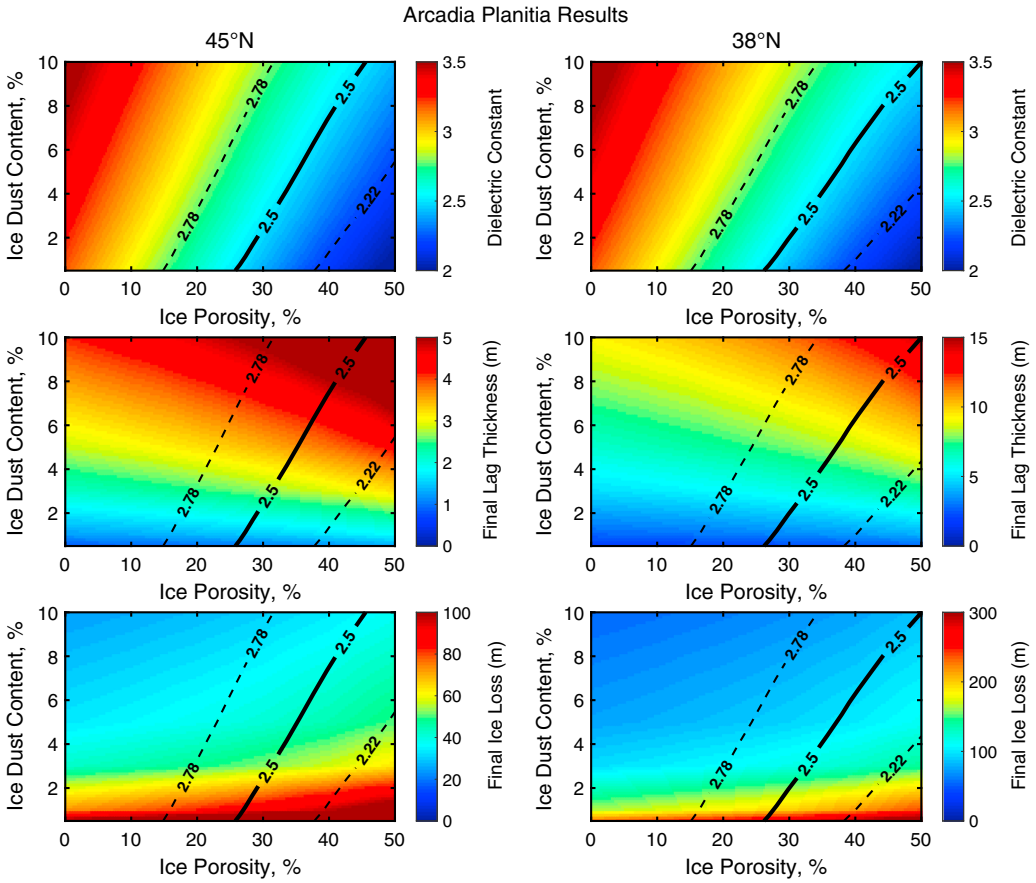

Figure 7. Plots of (top row) final dielectric constant, (middle row) lag thickness, and (bottom row) ice retreat for (left column) 45°N and (right column) 38°N for model runs in Arcadia Planitia (A = 0.23, TI = 196). The solid line is the average dielectric constant for Arcadia Planitia (2.5), and the dashed lines represent the upper and lower limit of the error bars of the dielectric constant from Bramson et al. (2015).

the thicknesses observed in this region, due to the Utopia deposit being a factor of 2–3 thicker than that of Arcadia. The higher average dielectric constant in Utopia Planitia suggests that this ice may require less porosity to be consistent with the observations; however, the error bars are larger, so these cases place weaker constraints on parameters than the Arcadia Planitia cases.

3.3. Contribution to the North Polar Layered Deposits

To quantify the contribution of ice lost from these deposits to the NPLD, we calculate approximate volumes of ice loss over time. For our volume calculations, we use the maximum areas reported for each regional deposit at present day (Table 1). For Arcadia Planitia, this area is calculated from a convex hull around the radar detections (Bramson et al., 2015). For Utopia Planitia, this area is the entire extent of the geomorphological unit on which the radar reflectors were identified (Stuurman et al., 2016; Kerrigan, 2013). However, there is uncertainty on the full extent of the deposits, as SHARAD cannot detect reflectors shallower than ~20–30 m, and we do not know how extensive the ice sheets could have been in the past. This means that the values we report here are not necessarily upper limits.

We divide the area for Arcadia Plantia (1,200,000 km^2) into three equal areas of 25 m (highest latitudes), 50 m (middle latitudes), and 120 m (lowest latitudes) of ice loss based on our nominal run (Figure 5) to calculate a volume of pure ice (0% porosity) lost in Arcadia Planitia over the last 21 Myr of ~52,300 km^3. Using the area of the geomorphological unit in Utopia Planitia (1,000,000 km^2), and ice retreat thicknesses that are twice as thick as those in Arcadia Planitia, we get an approximate ice loss of ~87,100 km^3 from Utopia Planitia. This yields a total ice volume lost from Arcadia Planitia and Utopia Planitia over the last 21 Myr of ~140,000 km^3.

The area of NPLD is 1.12×10^6 km^2, with a lower limit (assuming no flexure) on the volume of 1.14×10^6 km^3 (Smith et al., 2001). This means that retreat of the midlatitude deposits could have contributed ~12% of the

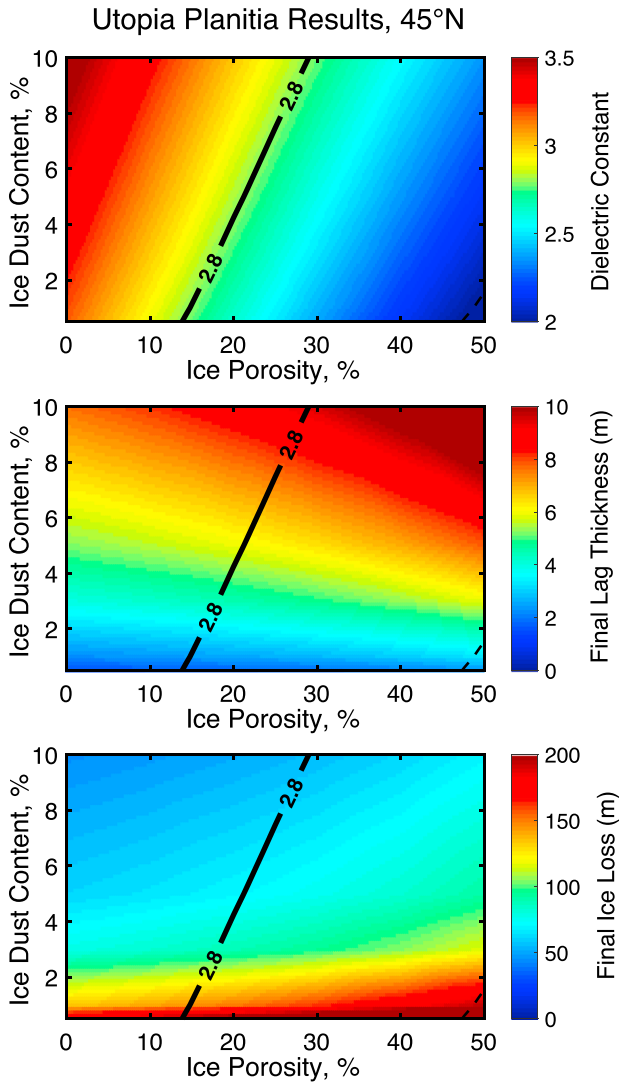

Figure 8. Plots of final (top) dielectric constant, (middle) lag thickness, and (bottom) ice retreat for model runs at 45°N in Utopia Planitia (A = 0.12, TI = 195). The solid line is the average dielectric constant for Utopia Planitia (2.8) with the upper limit of the error bar (3.6) outside of the plot and the lower limit of the dielectric constants error (2) in the bottom right corner. The dielectric constant values for Utopia Planitia are from Stuurman et al. (2016).

volume of ice of the NPLD (assuming 0% porosity), equating to 124 m of its thickness over 21 Myr if the NPLD are at least this age. Global climate models suggest that the accumulation of a northern ice cap may have initiated with the decrease in average insolation at the poles 4 Myr ago (Levrard et al., 2007). Using just the amount of ice that retreated in the last 4 Myr of our model gives a volume estimate ~50% lower, which suggests that these midlatitude deposits could have contributed ~6% of the volume of the NPLD since the drop in mean obliquity.

A widespread, recent accumulation package ("WRAP") within the polar layered deposits was identified in the SHARAD data and has been attributed to accumulation of ice since the end of the last Martian ice age ~370 ka (Smith et al., 2016). This unit was found to have a volume of 80,000 km^3 at the north pole and 7,000 km^3 at the south pole (Smith et al., 2016). Following the above calculations with the amount of ice that retreats in the last 370 kyr of our nominal model runs, we find that the volume of pure ice lost from the Arcadia Planitia and Utopia Planitia deposits in this timespan is ~2,883 km^3. Therefore, retreat of these two midlatitude excess ice reservoirs could have contributed ~3% of this most recent accumulation unit.

4. Densification of Martian Excess Ice

Our results suggest that midlatitude ice sheets would need to maintain substantial porosity (~25–35%) in the time since their emplacement. On Earth, buried snow densifies to the point that air bubbles are isolated from the atmosphere within timescales of roughly a few hundred years (Schwander et al., 1997). Here we model vapor diffusion through porous ice to explore the feasibility of retaining porosity in an ice sheet under Martian conditions for much longer timescales.

Densification of snow into firn and then dense ice on Earth likely happens orders of magnitude faster than on Mars (Arthern et al., 2000). The low temperatures, atmospheric pressures, accumulation rates, and gravity on Mars will contribute to longer densification times. Under dry conditions, the most important factor in the initial stages of densification from snow into firn is the settling of particles; for spherically shaped particles, packing experiments show that this process can reduce porosity to no less than 40% (corresponding density of 550 kg/m^3) (Cuffey & Paterson, 2010). Vapor diffusion then dominates and drives the intermediate stages of densification, contributing to growing "necks" between ice grains. Recrystallization and deformation change the shape and size of crystals to reduce stresses, occurring quicker under pressure, until density reaches ~730 kg/m^3. In the final stages, ice deformation takes over to close off air spaces from each other. At this point (density of ~830 kg/m^3), the firn has become glacial ice and additional reductions in porosity are due to compression and removal of air bubbles. Though important to ice densification on Earth, the effects of meltwater are likely much less important on Mars, especially during the cold-and-dry climate of the late Amazonian and at depths of only decameters, where overburden pressures are low. Brief peaks in surface temperature could aid in crystal coagulation and densification very near to the surface (the diurnal thermal skin depth of ice is tens of centimeters). However, this would only play a role very shortly after ice emplacement, as a low thermal inertia lag forms quickly, dampening the temperature variations experienced by the top of the ice sheet. Our understanding of firn densification processes is rooted in terrestrial experience, however, and other processes such as migration of water through thin surface films may be important over the longer timescales considered at Mars and require further investigation.

Under Mars' current climate, vapor transport has been found to dominate over ice-deformation mechanisms (Arthern et al., 2000). To test if intermediate porosities (values between that caused by compaction and the

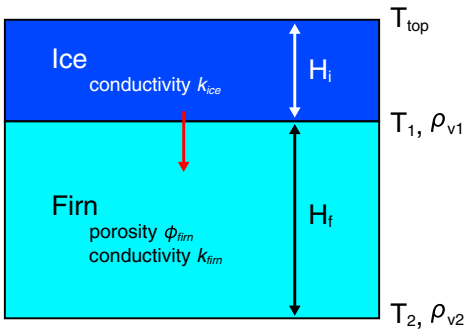

Figure 9. Diagram showing the structure of the vapor diffusion densification model. The red arrow indicates that the interface between layers moves downward as the dense ice layer thickens.

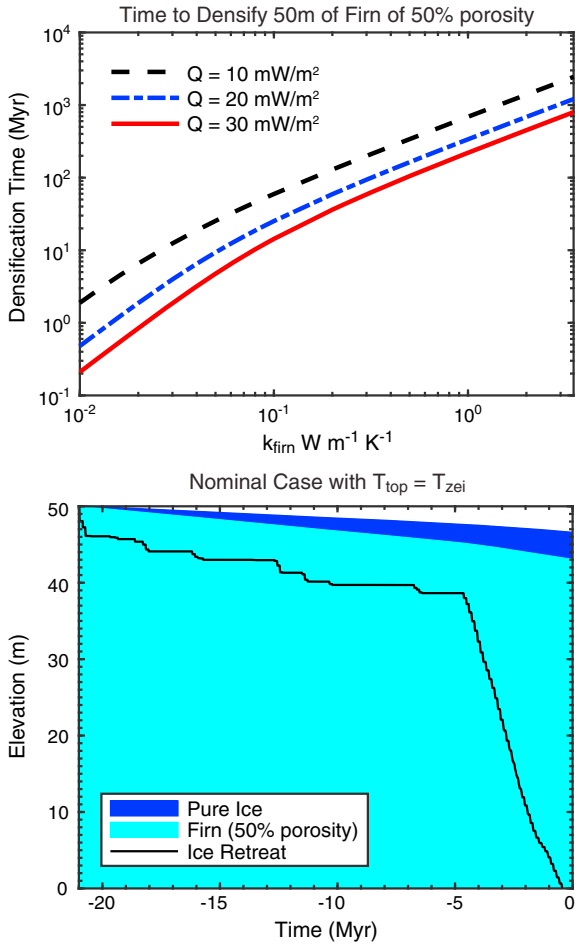

Figure 10. Results of modeling ice densification driven by vapor diffusion. (top) Relationship between densification time and conductivity of the firn for a constant ice table temperature of 205 K and three heat flux values. (bottom) Diagram showing the decrease in firn thickness and subsequent growth of the dense ice layer as vapor diffuses. T_{top} is set to temperatures at the excess ice interface from our nominal ice stability model over 21 Myr. Overplotted on this diagram is the ice retreat from sublimation that would occur in the same timespan.

sealing off of pores at high densities) are reasonable tens of millions of years after emplacement, we model vapor diffusion driven by temperature gradients through firn, similar to Mellon et al. (1997), which concerned the movement of vapor through porous regolith and interstitial ice. Here we use the term firn to simply refer to porous ice. We set the temperatures at the top (T_1) and bottom (T_2) of the firn layer to be the average excess ice interface temperatures ($T_{top} = T_{Z_{ei}}$) plus the geothermal gradient due to planetary heat flux, Q. This is shown in equation (8), where k is the thermal conductivity of pure ice (k_{ice}) or firn (k_{firn}), H_i is the thickness of ice, and H_f is the thickness of the firn. Corresponding saturation vapor densities (ρ_v) are calculated, and the difference between vapor densities at the top and bottom of the firn layer drives vapor diffusion from the bottom of the firn into the pore spaces at the top. This removes material from the bottom as a front of dense ice grows downward (Figure 9). We integrate over time to calculate a new thickness of the dense ice (H_i) and firn (H_f) layers (equations (9) and (10)).

$$T_1 = T_{top} + \frac{Q}{k_{ice}} H_i \quad \text{and} \quad T_2 = T_{top} + \frac{Q}{k_{ice}} H_i + \frac{Q}{k_{firn}} H_f \tag{8}$$

$$H_{f\_new} = \sqrt{{H_{f\_old}}^2 - \frac{2\, D_{ice}\, (\rho_{v2} - \rho_{v1})}{\phi_{firn}\,(1 - \phi_{firn})\rho_{ice}} (t_{new} - t_{old})} \tag{9}$$

$$H_{i\_new} = H_{i\_old} + (H_{f\_old} - H_{f\_new})(1 - \phi_{firn}) \tag{10}$$

We test a range of constant T_{top} values (195–215 K) for models spanning times longer than 21 Myr. For runs within this time frame of 21 Myr, we use the annual average temperature outputs at the excess ice interface from our nominal thermal model. We also assume that the firn is sealed off from the atmosphere by the densified top layer such that mass is conserved. We investigate the time needed for 50 m of 50% porosity firn to turn into pure ice via vapor diffusion, one of the main drivers of the intermediate stages of firn densification, especially on Mars (Arthern et al., 2000). This is an approximation, as vapor diffusion is inhibited when the pore spaces become isolated from each other at ~10% porosity (Arthern et al., 2000; Maeno & Ebinuma, 1983). The main factors that affect the amount of densification in this model are the heat flux, firn thermal conductivity, and vapor diffusivity (each discussed below), but, in general, we find timescales for complete densification of tens to hundreds of millions of years.

We use a nominal heat flux of 30 mW/m^2 (Fanale, 1976), although this is an upper limit for the late Amazonian and in the northern plains (Phillips et al., 2008; Plesa et al., 2016; Ruiz et al., 2008; Ruiz, López, & Dohm, 2010; Solomon et al., 2005). As the heat flux is likely smaller than this, Q = 30 mW/m^2 provides a conservative lower limit on densification time for any given k_{firn}. Figure 10 shows a plot of densification times versus conductivity for this heat flux as well as two smaller values (10 and 20 mW/m^2).

While thermal conductivity of ice is empirically dependent on temperature (Cuffey & Paterson, 2010), conductivity only ranges 3.23–3.05 W m^{-1} K^{-1} for the range of annual average temperatures at the excess ice interface within the last 21 Myr (~195–205 K). It therefore contributes negligibly to changing densification time; the relationship of conductivity to porosity is much more important. A linear relationship with porosity would mean that conductivity would drop from that of pure ice (3.2 W m^{-1} K^{-1}) to 1.6 W m^{-1} K^{-1} for 50% porosity, yielding a densification time of 360 Myr for a T_{top} of 205 K. Measurements of effective thermal conductivities of 30 terrestrial snow samples spanning a range of seasonal snow types

suggest a strong correlation between thermal conductivity and snow density (Calonne et al., 2011). The relationship of Calonne et al. (2011), shown in equation (11), matches closely with that proposed in a comprehensive data review by Yen (1981). For a porosity of ~50% (density ~458 kg/m^3), the fit from Calonne et al. (2011) yields a conductivity of 0.493 W m^{-1} K^{-1}. The Van Dusen (1929) formula for conductivity (equation (4)) also has a nonlinear dependence on porosity and in most cases is expected to be a lower limit. This formula yields $k \sim 0.43$ W m^{-1} K^{-1} for the same density, which we take to be our nominal value. Cassanelli and Head (2015) base their lower limit of conductivity on an expression from Carr and Head (2003). Using the Carr and Head (2003) formula (equation (12)) as an extreme lower limit would yield a conductivity of 0.26 W m^{-1} K^{-1} and densification time of 50 Myr.

$$k = \left(2.5\times10^{-6}\right)\rho^2 - \left(1.23\times10^{-4}\right)\rho + 0.024 \tag{11}$$

$$\log(k) = 0.4 + 2.9\ \log(\rho) \tag{12}$$

The effective water vapor diffusion coefficient in snow on Earth has been found to be on the order of 10^{-5} to 10^{-4} m^2/s (Sokratov & Maeno, 2000). We use a value on the upper extreme of terrestrial firn diffusivities (nominal D_{ice} of 10^{-4} m^2/s) to account for the lower pressure on Mars; this value is also on the same order as the diffusion coefficient of other porous materials under simulated Mars surface conditions (Hudson et al., 2007). The diffusive flux is linearly dependent on the diffusion coefficient; thus, if the diffusion coefficient of vapor through Martian firn is higher than this nominal value by an order of magnitude, the densification timescales would correspondingly decrease by an order of magnitude from those reported here.

Using all of our nominal conditions described above and our modeled temperatures, the dense ice layer grows to a thickness of 3.5 m, while 43 m of the column remains as porous firn over the last 21 Myr. Under these conditions, but with a T_{top} of 205 K, 50 m of ice would take 86 Myr to densify completely. The rate of densification is small compared to the rate of ice loss over this same time frame (~50 m ice retreat), as shown in Figure 10. As the retreat will occur from the top dense ice layer, the bottom porous layer will dominate what is left of the column leading to the low dielectric constants observed. As such, we would not necessarily expect complete densification of the remaining ice sheet over relevant timescales.

5. Discussion

5.1. Carbon Dioxide Clathrates

Although our densification experiment above (section 4) suggests that it could be possible to maintain porosity in the ice, one alternative possibility to explain the low dielectric constants of these northern midlatitude deposits could be a significant amount of buried carbon dioxide clathrates in these regions. The dielectric properties of carbon dioxide clathrates are not well characterized. However, they contain a nonpolar guest molecule in a type I lattice structure similar to that of N_2 clathrates, which have an ε_r of ~2.85 (Nunes & Phillips, 2006). Replacing ε_{ice} with this value in the calculation of bulk dielectric constant would lower the required porosity of the deposit. The CO_2 gas pressure needed to form clathrate at 205 K is ~0.5 bar (Mellon, 1996). Pore-filling atmospheric CO_2 in the firn would initially be at atmospheric pressure; however, as firn densifies the pore space is reduced and the gas can become pressurized. The maximum amount of clathrate that could be formed in this way is limited though. For an ~50 m thick column of material with 50% porosity, the total mass of CO_2 gas in the pores will be less than 1 kg. If completely converted, this would produce only ~20 kg of clathrates compared to the >20 metric tons of water ice in the column. Therefore, it is unlikely that carbon dioxide clathrates make a substantial contribution to the midlatitude deposits we are discussing here.

5.2. Latitudinal Trends on Lag Growth and Excess Ice Retreat

In our results, we find more retreat, and thus growth of a thicker lag deposit, at lower latitudes. This trend is expected since the depth to stable ice increases as you move equatorward and suggests that we should observe a latitudinal trend in lag thickness. The distribution of ice depth versus latitude based on recent ice exposing impacts (Dundas et al., 2014) indeed suggests that there is a latitudinal trend in lag thickness, though their estimation of excavation depth suggests that the lag thicknesses we model may be larger by a factor of a few. For example, in the 38°N Arcadia Planitia case, our nominal dust content of 3% and ice porosity of 30% yields a lag thickness of ~5 m. But some craters at this latitude expose relatively pure ice within the upper meter of the surface (Dundas et al., 2014). It is possible that the excess ice exposed by these craters

is more shallowly and recently sourced, such as ice lens formation within a pore-filling ice layer (Sizemore, Zent, & Rempel, 2015), similar to that proposed for the excess ice excavated at Phoenix (Mellon et al., 2009). If such a layer is pervasive across the midlatitude and high latitude of Mars, it could significantly affect the diffusive exchange of water vapor between the deeper subsurface and the atmosphere.

If the excess ice exposed by the recent craters is the top of the excess ice deposit detected in the radar studies modeled here, then cases of higher atmospheric water vapor content, lower regolith vapor diffusivity, and/or lower dust content in the ice are required. We find that an order of magnitude difference in regolith diffusivity has an effect of changing the total ice retreats and lag thicknesses by a factor of ~3. However, experiments show that it is difficult to achieve this significant reduction of D without invoking a low-diffusivity barrier such as a duricrust or salt-cemented sediments (Hudson et al., 2007). Concentrating atmospheric water vapor at the surface with $H_c/H = 0.5$, the final lag thickness produced at 38°N is 1.13 m for an ice porosity of 25%, dust content of 1%, and $D = 1 \times 10^{-4}$ m^2/s. If we lower H_c/H to 0.4, this lag deposit can be further restricted to only 1.06 m thick after 21 Myr. Both of these cases yield dielectric constants of 2.5, consistent with the radar observations.

In the case of $H_c/H \geq 0.5$, pore-filling ice is not currently stable at 38°N. However, our model suggests that pore-filling ice is stable at this latitude, with an equilibrium depth of 8 cm, under present conditions if atmospheric water vapor was further concentrated to $H_c/H = 0.4$. Additional observations of the stratigraphy in the upper meters of the surface (which current orbital radars at Mars are not sensitive to) will help put additional constraints on the atmospheric water vapor contents, vapor diffusivity, and ice properties.

5.3. Additional Obliquity Effects

Mars' orbit undergoes large oscillations, having undergone multiple dips into very low obliquities (<15°) in the last 5 Myr. During these times, the poles receive less insolation and it is predicted that the carbon dioxide atmosphere collapses into permanent solid CO_2 deposits, although complete collapse is impossible unless these polar deposits are at 0 K. At these times, the remaining argon and nitrogen will provide ~0.25 mbar of atmospheric pressure (Kreslavsky & Head, 2005). When the pressures are low, however, the mean free path of an atmospheric molecule will be large relative to the size of the pore space. In this "Knudsen" regime, the gas conductivity (and thus the bulk thermal conductivity) of dry regolith will be smaller (Piqueux & Christensen, 2009a), more effectively insulating the ice below. Lower conductivity soils will decrease ice sublimation rates, making the ice more stable. However, the lower atmospheric pressure will also increase the vapor diffusion coefficient. In the Knudsen regime, the vapor diffusion coefficient becomes independent of pressure, and D approaches 9.8×10^{-4} m^2/s (Hudson et al., 2007). The transition pressure between these two regimes was found to be 398 Pa, although the bulk of diffusion even at 50 Pa may be in a transition flow between the two regimes for a given distribution of pore sizes (Hudson et al., 2007). The above effects may be important for ice stability and lag generation at low obliquities and are not accounted for in our model. Further work is needed to establish the fate of midlatitude ice during times of atmospheric collapse; however, these extreme dips in obliquity represent a very small fraction of the past 21 Myr we simulated.

At high obliquities, ice is stable in the midlatitudes and could even undergo additional accumulation, either through snowfall onto the surface or pore ice accumulation within the ice sheet. In this paper, we consider the simplified case where we start with a preexisting ice sheet at the midlatitudes at the beginning of Laskar et al.'s (2004) orbital solution in order to assess the maximum retreat that could occur. High obliquity excursions throughout the last 21 Myr, especially before ~4 Ma, could have additionally deposited ice in the midlatitudes (e.g., Madeleine et al., 2009). However, the amount of additional ice emplacement would have to be relatively small (<20 m) as to avoid burying the expanded secondary craters mapped by Viola et al. (2015) in the tens of millions of years since crater formation. Additional ice accumulation in the midlatitudes would only make thick (tens of meters) ice sheets easier to explain, as this ice would be the first to sublimate as the obliquity drops. This would suggest that there may also be layering of multiple sublimation lags in these midlatitude deposits. Evidence of possible layering within this ice sheet exists in several of the terraced craters in Arcadia Planitia, which exhibit an additional shallower and less prominent terrace, perhaps at the interface between two such ice layers (Bramson et al., 2015). Future studies with higher-resolution RADAR sounder data or imaging of recently eroded cross sections through midlatitude ice deposits may resolve this. While beyond the scope of this paper, future studies could account for additional ice accumulation/sublimation and lag growth during high obliquities to establish the net effect of additional high-obliquity accumulation scenarios on midlatitude ice sheets.

5.4. Comparison to Previous Models

Previous work by Schorghofer and Forget (2012) predict that thick ice sheets in the Martian midlatitudes would be geologically recent and actively retreating under current atmospheric conditions. This is consistent with the model of Martian ice ages proposed by Head et al. (2003), which predicts that the meter-thick ice-rich latitude-dependent mantle is $<$2.1 Myr old and currently being degraded. Based on our model results, we also conclude that ice sheets in the midlatitudes have been retreating in the recent past (last few Myr), including present day, during these low obliquity "interglacial" periods. However, our results as well as the observations from Viola et al. (2015) suggest that the decameter-thick ice sheets discovered in Arcadia Planitia and Utopia Planitia could be older than previously thought.

The results of the ice stability model of Schorghofer and Forget (2012) show that an ~4.5 Myr old ice sheet that is 30 m thick would not have survived at these latitudes to the present day. We also calculate $>$30 m of ice loss for our nominal case at 45°N. However, our initial condition allows ice of infinite thickness, and it is because of this we reach a different conclusion.

Because our model does not stop at a finite amount of ice loss, we are also able to explore longer timescales (specifically 21–4.5 Ma). We find that the higher average obliquities before 4.5 Ma so commonly yield stable ice conditions that this older time frame is less important for retreat of ice sheets than the most recent ~4 Myr. Therefore, we additionally conclude that if an ice sheet is thick enough to survive the last 4.5 Myr, it can likely be 21 Myr old, or even older.

In contrast to Schorghofer and Forget (2012), our retreat rates include the effect of porosity. For our nominal case at 45°N, the inclusion of porosity increases the final ice retreat by ~23% (43 m of retreat for an ice porosity of 0% versus 53 m with a porosity of 30%). The maximum porosity we tested, 50%, yields 64 m of retreat —a 49% increase from the 0% porosity case. The inclusion of this parameter contributes less than an order of magnitude to the estimated ice volume lost compared to models that assume a pure ice slab and is not the main reason for the difference in conclusions between this and previous work.

We conclude that there is no discrepancy between our model and previous work, and the initial condition (infinite ice versus 30 m thick ice) is the main contributor to reaching different conclusions.

6. Conclusions

We simulate the evolution of an excess ice sheet in the midlatitudes of Mars, insulated by a growing lag deposit, over 21 Myr of Martian orbital parameters in order to investigate if it is reasonable to expect Martian midlatitude ice to persist for orders of magnitude longer than the obliquity cycles that drive pore-filling ice processes. We find combinations of ice porosity and dust contents that yield ice retreat on the same order of magnitude as the thicknesses of ice presently observed in Arcadia Planitia and Utopia Planitia, suggesting that tens of Myr-old, decameters-thick ice sheets could be preserved until today if they formed ~2–3 times as thick and had small, but nonzero, dust content. To match observed dielectric constants (Bramson et al., 2015; Stuurman et al., 2016), we need to invoke porosities of at least ~25–35% in the ice layer presently for volumetric dust contents of ~1–5%. While snowpacks on Earth generally turn to firn and densify rapidly, we show that these levels of porosities may be maintained for orders of magnitude longer timescales under Martian conditions (lower accumulation rates, temperatures, and pressures compared to Earth). Modeling of geothermally driven vapor diffusion through porous ice suggests that water vapor should migrate through and recondense into a top layer of dense ice on timescales longer than that of ice retreat. This means that retreat will come from the upper layers, leaving behind the underlying porous ice. Our results suggest that thick deposits of midlatitude firn with low dust contents are a long-lived feature of Amazonian Mars. Superposed craters show that these deposits are at least tens of millions of years old. Our retreat models suggest minimal loss when obliquity is high prior to 4 Ma. Given that the most probable value of obliquity over the Amazonian is 41.8° (Laskar et al., 2004), these firn deposits may be substantially older. The ice loss from these deposits over the past 4 Myr could contribute ~62 m to the construction of the NPLD or on the order of 10% if the NPLD is older than 4–5 Myr.

Acknowledgments
A.M.B. was supported by the National Science Foundation (NSF) Graduate Research Fellowship Program under grant DGE-1143953 and a NASA Earth and Space Sciences Fellowship (NESSF) under grant NNX16AP09H. J.B. was funded under NASA Mars Data Analysis Program (MDAP) award NNX15AM62G. We thank Norbert Schörghofer for insightful discussions and Cassie Stuurman for the Utopia Planitia radar reflector data plotted in Figure 1b. Observational data used in this study (including MOLA topography maps and TES thermal inertias and albedos) are available to the public on the Planetary Data System. Input and output files of the thermal model results in this study are available at https://doi.org/10.6084/m9.figshare.5471539.v1. The authors thank Hanna Sizemore, Roberto Orosei, and an anonymous reviewer for their helpful comments.

References

Aharonson, O., & Schorghofer, N. (2006). Subsurface ice on Mars with rough topography. *Journal of Geophysical Research*, *111*, E11007. https://doi.org/10.1029/2005JE002636

Arthern, R. J., Winebrenner, D. P., & Waddington, E. D. (2000). Densification of water ice deposits on the residual north polar cap of Mars. *Icarus*, *144*(2), 367–381. https://doi.org/10.1006/icar.1999.6308

Bramson, A. M., Byrne, S., Putzig, N. E., Sutton, S., Plaut, J. J., Brothers, T. C., & Holt, J. W. (2015). Widespread excess ice in Arcadia Planitia, Mars. *Geophysical Research Letters*, *42*(16), 6566–6574. https://doi.org/10.1002/2015GL064844

Bryson, K. L., Chevrier, V., Sears, D. W. G., & Ulrich, R. (2008). Stability of ice on Mars and the water vapor diurnal cycle: Experimental study of the sublimation of ice through a fine-grained basaltic regolith. *Icarus*, *196*(2), 446–458. https://doi.org/10.1016/j.icarus.2008.02.011

Calonne, N., Flin, F., Morin, S., Lesaffre, B., Roscoat, S. R. D., & Geindreau, C. (2011). Numerical and experimental investigations of the effective thermal conductivity of snow. *Geophysical Research Letters*, *38*, L23501. https://doi.org/10.1029/2011GL049234

Carr, M. H., & Head, J. W. (2003). Basal melting of snow on early Mars: A possible origin of some valley networks. *Geophysical Research Letters*, *30*(24), 2245. https://doi.org/10.1029/2003GL018575

Cassanelli, J. P., & Head, J. W. (2015). Firn densification in a Late Noachian "icy highlands" Mars: Implications for ice sheet evolution and thermal response. *Icarus*, *253*, 243–255. https://doi.org/10.1016/j.icarus.2015.03.004

Chamberlain, M. A., & Boynton, W. V. (2007). Response of Martian ground ice to orbit-induced climate change. *Journal of Geophysical Research*, *112*, E06009. https://doi.org/10.1029/2006JE002801

Chevrier, V., Sears, D. W. G., Chittenden, J. D., Roe, L. A., Ulrich, R., Bryson, K. L., … Hanley, J. (2007). Sublimation rate of ice under simulated Mars conditions and the effect of layers of mock regolith JSC Mars-1. *Geophysical Research Letters*, *34*, L02203. https://doi.org/10.1029/2006GL028401

Christensen, P. R., Bandfield, V. E. H., Ruff, S. W., Kieffer, H. H., Titus, T. N., … Greenfield, M. (2001). Mars Global Surveyor Thermal Emission Spectrometer experiment: Investigation description and surface science results. *Journal of Geophysical Research*, *106*(E10), 23,823–23,871. https://doi.org/10.1029/2000JE001370

Crank, J., & Nicolson, P. (1947). A practical method for numerical evaluation of solutions of partial differential equations of the heat-conduction type. *Mathematical Proceedings of the Cambridge Philosophical Society*, *43*(01), 50–67. https://doi.org/10.1017/S0305004100023197

Cuffey, K. M., & Paterson, W. S. B. (2010). *Physics of Glaciers*, (4th ed.). Burlington, MA: Butterworth-Heinemann/Elsevier.

Dundas, C. M., Byrne, S., & McEwen, A. S. (2015). Modeling the development of Martian sublimation thermokarst landforms. *Icarus*, *262*, 154–169. https://doi.org/10.1016/j.icarus.2015.07.033

Dundas, C. M., Byrne, S., McEwen, A. S., Mellon, M. T., Kennedy, M. R., Daubar, I. J., & Saper, L. (2014). HiRISE observations of new impact craters exposing Martian ground ice. *Journal of Geophysical Research, Planets*, *119*(1), 109–127. https://doi.org/10.1002/2013JE004482

Fanale, F. P. (1976). Martian volatiles: Their degassing history and geochemical fate. *Icarus*, *28*(2), 179–202. https://doi.org/10.1016/0019-1035(76)90032-4

Feldman, W. C., Pathare, A., Maurice, S., Prettyman, T. H., Lawrence, D. J., Milliken, R. E., & Travis, B. J. (2011). Mars Odyssey neutron data: 2. Search for buried excess water ice deposits at nonpolar latitudes on Mars. *Journal of Geophysical Research*, *116*, E11009. https://doi.org/10.1029/2011JE003806

Head, J. W., Mustard, J. F., Kreslavsky, M. A., Milliken, R. E., & Marchant, D. R. (2003). Recent ice ages on Mars. *Nature*, *426*(6968), 797–802. https://doi.org/10.1038/nature02114

Hess, S. L., Ryan, J. A., Tillman, J. E., Henry, R. M., & Leovy, C. B. (1980). The annual cycle of pressure on Mars measured by Viking landers 1 and 2. *Gephysical Research Letters*, *7*(3), 197–200. https://doi.org/10.1029/GL007i003p00197

Holt, J. W., Safaeinili, A., Plaut, J. J., Head, J. W., Phillips, R. J., Seu, R., … Gim, Y. (2008). Radar sounding evidence for buried glaciers in the southern mid-latitudes of Mars. *Science*, *322*(5905), 1235–1238. https://doi.org/10.1126/science.1164246

Hudson, T. L., Aharonson, O., Schorghofer, N., Farmer, C. B., Hecht, M. H., & Bridges, N. T. (2007). Water vapor diffusion in Mars subsurface environments. *Journal of Geophysical Research*, *112*, E05016. https://doi.org/10.1029/2006JE002815

Johansen, O. (1975). Thermal conductivity of soils, PhD thesis, University of Trondheim, Trondheim, Norway.

Kerrigan, M. (2013). The Periglacial Landscape of Utopia Planitia; Geologic Evidence for Recent Climate Change on Mars, MS thesis, Department of Earth Sciences, University of Western Ontario, London, Ontario, Canada.

Kieffer, H. H. (2013). Thermal model for analysis of Mars infrared mapping. *Journal of Geophysical Research: Planets*, *118*, 451–470. https://doi.org/10.1029/2012JE004164

Kieffer, H. H., Martin, T. Z., Peterfreund, A. R., Jakosky, B. M., Miner, E. D., & Palluconi, F. D. (1977). Thermal and albedo mapping of Mars during the Viking primary mission. *Journal of Geophysical Research*, *82*(28), 4249–4291. https://doi.org/10.1029/JS082i028p04249

Kreslavsky, M. A., & Head, J. W. (2005). Mars at very low obliquity: Atmospheric collapse and the fate of volatiles. *Geophysical Research Letters*, *32*, L1220. https://doi.org/10.1029/2005GL022645

Laskar, J., Correia, A. C. M., Gastineau, M., Joutel, F., Levrard, B., & Robutel, P. (2004). Long term evolution and chaotic diffusion of the insolation quantities of Mars. *Icarus*, *170*(2), 343–364. https://doi.org/10.1016/j.icarus.2004.04.005

Levrard, B., Forget, F., Montmessin, F., & Laskar, J. (2007). Recent formation and evolution of northern Martian polar layered deposits as inferred from a global climate model. *Journal of Geophysical Research*, *112*, E06012. https://doi.org/10.1029/2006JE002772

Madeleine, J.-B., Forget, F., Head, J. W., Levrard, B., Montmessin, F., & Millour, E. (2009). Amazonian northern mid-latitude glaciation on Mars: A proposed climate scenario. *Icarus*, *203*(2), 390–405. https://doi.org/10.1016/j.icarus.2009.04.037

Maeno, N., & Ebinuma, T. (1983). Pressure sintering of ice and its implication to the densification of snow at polar glaciers and ice sheets. *The Journal of Physical Chemistry*, *87*(21), 4103–4110. https://doi.org/10.1021/j100244a023

Mellon, M. T. (1996). Limits on the CO_2 content of the Martian polar deposits. *Icarus*, *124*(1), 268–279. https://doi.org/10.1006/icar.1996.0203

Mellon, M. T., Arvidson, R. E., Sizemore, H. G., Searls, M. L., Blaney, D. L., Cull, S., … Zent, A. P. (2009). Ground ice at the Phoenix landing site: Stability state and origin. *Journal of Geophysical Research*, *114*, E00E07. https://doi.org/10.1029/2009JE003417

Mellon, M. T., Feldman, W. C., & Prettyman, T. H. (2004). The presence and stability of ground ice in the southern hemisphere of Mars. *Icarus*, *169*(2), 324–340. https://doi.org/10.1016/j.icarus.2003.10.022

Mellon, M. T., Jakosky, B. M., Kieffer, H. H., & Christensen, P. R. (2000). High-resolution thermal inertia mapping from the Mars Global Surveyor Thermal Emission Spectrometer. *Icarus*, *148*(2), 437–455. https://doi.org/10.1006/icar.2000.6503

Mellon, M. T., Jakosky, B. M., & Postawko, S. E. (1997). The persistence of equatorial ground ice on Mars. *Journal of Geophysical Research*, *102*(E8), 19,357–19,369. https://doi.org/10.1029/97JE01346

Nunes, D. C., & Phillips, R. J. (2006). Radar subsurface mapping of the polar layered deposits on Mars. *Journal of Geophysical Research*, *111*, E06S21. https://doi.org/10.1029/2005JE002609

Phillips, R. J., Zuber, M. T., Smrekar, S. E., Mellon, M. T., Head, J. W., Tanaka, K. L., … Marinangeli, L. (2008). Mars north polar deposits: Stratigraphy, age, and geodynamical response. *Science*, *320*(5880), 1182–1185. https://doi.org/10.1126/science.1157546

Piqueux, S., & Christensen, P. R. (2009a). A model of thermal conductivity for planetary soils: 1. Theory for unconsolidated soils. *Journal of Geophysical Research*, *114*, E09005. https://doi.org/10.1029/2008JE003308

Piqueux, S., & Christensen, P. R. (2009b). A model of thermal conductivity for planetary soils: 2. Theory for cemented soils. *Journal of Geophysical Research*, *114*, E09006. https://doi.org/10.1029/2008JE003309

Plesa, A.-C., Grott, M., Tosi, N., Breuer, D., Spohn, T., & Wieczorek, M. A. (2016). How large are present-day heat flux variations across the surface of Mars? *Journal of Geophysical Research: Planets*, *121*, 2386–2403. https://doi.org/10.1002/2016JE005126

Putzig, N., & Mellon, M. T. (2007). Thermal behavior of horizontally mixed surfaces on Mars. *Icarus*, *191*(1), 52–67. https://doi.org/10.1016/j.icarus.2007.03.022

Putzig, N., Mellon, M. T., Kretke, K., & Arvidson, R. E. (2005). Global thermal inertia and surface properties of Mars from the MGS mapping mission. *Icarus*, *173*(2), 325–341. https://doi.org/10.1016/j.icarus.2004.08.017

Ruiz, J., Fernández, C., Gomez-Ortiz, D., Dohm, J. M., López, V., & Tejero, R. (2008). Ancient heat flow, crustal thickness, and lithospheric mantle rheology in the Amenthes region, Mars. *Earth and Planetary Science Letters*, *270*(1-2), 1–12. https://doi.org/10.1016/j.epsl.2008.02.015

Ruiz, J., López, V., & Dohm, J. M. (2010). The present-day thermal state of Mars. *Icarus*, *207*(2), 631–637. https://doi.org/10.1016/j.icarus.2010.01.016

Schorghofer, N. (2007). Theory of ground ice stability in sublimation environments. *Physical Review E*, *75*(4), 041201. https://doi.org/10.1103/PhysRevE.75.041201

Schorghofer, N. (2010). Fast numerical method for growth and retreat of subsurface ice on Mars. *Icarus*, *208*(2), 598–607. https://doi.org/10.1016/j.icarus.2010.03.022

Schorghofer, N., & Aharonson, O. (2005). Stability and exchange of subsurface ice on Mars. *Journal of Geophysical Research*, *110*, E05003. https://doi.org/10.1029/2004JE002350

Schorghofer, N., & Forget, F. (2012). History and anatomy of subsurface ice on Mars. *Icarus*, *220*(2), 1112–1120. https://doi.org/10.1016/j.icarus.2012.07.003

Schwander, J., Sowers, T., Barnola, J.-M., Blunier, T., Fuchs, A., & Malaizé, B. (1997). Age scale of the air in the summit ice: Implication for glacier-interglacial temperature change. *Journal of Geophysical Research*, *102*(D16), 19,483–19,493. https://doi.org/10.1029/97JD01309

Siegler, M., Aharonson, O., Carey, E., Choukroun, M., Hudson, T., Schorghofer, N., & Xu, S. (2012). Measurements of thermal properties of icy Mars regolith analogs. *Journal of Geophysical Research*, *117*, E03001. https://doi.org/10.1029/2011JE003938

Sizemore, H. G., & Mellon, M. T. (2008). Laboratory characterization of the structural properties controlling dynamical gas transport in Mars-analog soils. *Icarus*, *197*(2), 606–620. https://doi.org/10.1016/j.icarus.2008.05.013

Sizemore, H. G., Zent, A. P., & Rempel, A. W. (2015). Initiation and growth of Martian ice lenses. *Icarus*, *251*, 191–210. https://doi.org/10.1016/j.icarus.2014.04.013

Smith, D. E., Zuber, M. T., Frey, H. V., Garvin, J. B., Head, J. W., Muhleman, D. O., … Sun, X. (2001). Mars Orbiter Laser Altimeter: Experiment summary after the first year of global mapping of Mars. *Journal of Geophysical Research*, *106*, 23,689–23,722. https://doi.org/10.1029/2000JE001364

Smith, I. B., Putzig, N. E., Holt, J. W., & Phillips, R. J. (2016). An ice age recorded in the polar deposits of Mars. *Science*, *352*(6289), 1075–1078. https://doi.org/10.1126/science.aad6968

Sokratov, S. A., & Maeno, N. (2000). Effective water vapor diffusion coefficient of snow under a temperature gradient. *Water Resources Research*, *36*(5), 1269–1276. https://doi.org/10.1029/2000WR900014

Solomon, S. C., Aharonson, O., Aurnou, J. M., Banerdt, W. B., Carr, M. H., Dombard, A. J., … Zuber, M. T. (2005). New perspectives on ancient Mars. *Science*, *307*(5713), 1214–1220. https://doi.org/10.1126/science.1101812

Stillman, D. E., Grimm, R. E., & Dec, S. F. (2010). Low-frequency electrical properties of ice-silicate mixtures. *The Journal of Physical Chemistry B*, *114*(18), 6065–6073. https://doi.org/10.1021/jp9070778

Stuurman, C. M., Osinski, G. R., Holt, J. W., Levy, J. S., Brothers, T. C., Kerrigan, M., & Campbell, B. A. (2016). SHARAD detection and characterization of subsurface water ice deposits in Utopia Planitia, Mars. *Geophysical Research Letters*, *43*(18), 9484–9491. https://doi.org/10.1002/2016GL070138

Van Dusen, M. S. (1929). Thermal conductivity of non-metallic solids. In E. W. Washburn (Ed.), *International Critical Tables of Numerical Data. Physics, Chemistry and Technology* (Vol. 5, pp. 216–217). McGraw Hill, New York.

Vasavada, A. R., Paige, D. A., & Wood, S. E. (1999). Near-surface temperatures on Mercury and the Moon and the stability of polar ice deposits. *Icarus*, *141*(2), 179–193. https://doi.org/10.1006/icar.1999.6175

Viola, D., McEwen, A. S., Dundas, C. M., & Byrne, S. (2015). Expanded secondary craters in the Arcadia Planitia region, Mars: Evidence for tens of Myr-old shallow subsurface ice. *Icarus*, *248*, 190–204. https://doi.org/10.1016/j.icarus.2014.10.032

Wechsler, A. E., Glaser, P. E., & Fountain, J. A. (1972). Thermal properties of granulated materials. In J. W. Lucas (Ed.), *Thermal Characteristics of the Moon* (pp. 215–241). Cambridge, MA: MIT Press.

Wilson, J. T., Eke, V. R., Massey, R. J., Elphic, R. C., Feldman, W. C., Maurice, S., & Teodoro, L. F. A. (2018). Equatorial locations of water on Mars: Improved resolution maps based on Mars Odyssey Neutron Spectrometer data. *Icarus*, *299*, 148–160. https://doi.org/10.1016/j.icarus.2017.07.028

Yen, Y.-C. (1981). Review of thermal properties of snow, ice, and sea ice, CRREL report 81-10, Cold Regions Research and Engineering Laboratory, Hanover, NH.